Jahn-Teller effect in tetrahedral symmetry: Large-amplitude tunneling motion and rovibronic structure of C H 4 + and C D 4 +

H. J. Wörner, X. Qian, and F. Merkt

Citation: The Journal of Chemical Physics **126**, 144305 (2007); doi: 10.1063/1.2712840
View online: http://dx.doi.org/10.1063/1.2712840
View Table of Contents: http://scitation.aip.org/content/aip/journal/jcp/126/14?ver=pdfcov
Published by the AIP Publishing

Jahn-Teller effect in tetrahedral symmetry: Large-amplitude tunneling motion and rovibronic structure of CH_4^+ and CD_4^+

H. J. Wörner, X. Qian,[a] and F. Merkt
Laboratorium für Physikalische Chemie, ETH-Zürich, 8093 Zürich, Switzerland

(Received 3 January 2007; accepted 6 February 2007; published online 10 April 2007)

The energy level structures of the ground vibronic states of $^{12}CH_4^+$, $^{13}CH_4^+$, and $^{12}CD_4^+$ have been measured by pulsed-field-ionization zero-kinetic-energy photoelectron spectroscopy. The nuclear spin symmetries of the tunneling-rotational levels have been determined in double-resonance experiments via selected rotational levels of the $v_3=1$ and $v_3=2$ vibrational levels of the $\tilde{X}\,^1A_1$ ground state of CH_4. The energy level structures of $^{12}CH_4^+$, $^{13}CH_4^+$, and $^{12}CD_4^+$ have been analyzed with an effective tunneling-rotational Hamiltonian. The analysis together with a group theoretical treatment of the $T\otimes(e+t_2)$ Jahn-Teller effect in the $T_d(M)$ group prove that the equilibrium geometry of $^{12}CH_4^+$, $^{13}CH_4^+$, and $^{12}CD_4^+$ has C_{2v} symmetry and characterize the pseudorotational dynamics in these fluxional cations. The tunneling behavior is discussed in terms of the relevant properties of the potential energy surface, some of which have been recalculated at the CCSD(T)/cc-pVTZ level of *ab initio* theory. © *2007 American Institute of Physics*. [DOI: 10.1063/1.2712840]

I. INTRODUCTION

The present report describes the results of recent experimental and theoretical investigations of the rovibronic structures of CH_4^+ and CD_4^+ which have provided the first complete assignment of the level structure of these cations at low energies. A brief account of the analysis of the CH_4^+ spectra has been given in Ref. 1. Innovations in experimental and theoretical procedures were required to achieve this goal. Experimentally, we have implemented double-resonance excitation techniques combining sources of vacuum-ultraviolet (VUV) and infrared (IR) radiation to experimentally assign the nuclear spin symmetry of the observed ionic levels. Theoretically, a tunneling treatment adequate to describe the complex topological properties of the potential energy surface of CH_4^+ has been developed and extended to include end-over-end rotation of the molecule.

The methane radical cation CH_4^+ is of fundamental importance in chemistry. It plays a role in the chemistry of interstellar clouds and planetary atmospheres. In mass spectrometry it is commonly used as reagent in chemical ionization. The ion-molecule chemistry of CH_4^+ is very rich, leading to other fundamental molecular ions such as CH_5^+ and $C_2H_5^+$. So far, CH_4^+ has not been detected by spectroscopic methods because neither its structure nor its transition frequencies were precisely known.

The methane cation is the simplest organic cation possessing a threefold degenerate electronic ground state which makes it the prototypical system for studies of the Jahn-Teller (JT) effect in the cubic point groups. Despite many previous studies, hardly any high-resolution experimental information is available on the JT effect in tetrahedral symmetry. The methane cation is subject to a particularly strong JT effect with a stabilization energy of 1.5 eV. The potential energy surface is pathologically flat near the minimum, and the cation is highly fluxional in its ground electronic state, the hydrogen atoms exchanging on a subnanosecond time scale. The investigation of the rovibronic structure thus offers the opportunity to fully characterize the JT effect and to deepen the current understanding of the dynamics of fluxional molecules. With only nine electrons, the methane cation can serve as a test for *ab initio* quantum chemical calculations and full-dimensional calculations of its nuclear dynamics.[2,3]

Studies by electron paramagnetic resonance[4,5] have proven that the protons in CH_4^+ exchange within the experimental time scale and that the hydrogen and deuterium atoms in $CH_2D_2^+$ occupy different positions. These observations were interpreted in terms of a C_{2v} equilibrium structure of the methane cation. A group theoretical analysis of the anomalous temperature dependence of the electron spin resonance spectra of CH_4^+ (Ref. 6) identified two molecular symmetry groups (A_4 and T_4) that are consistent with the observed spectra, but no further restrictions could be made. The vibronic structure has been partially resolved by He I photoelectron spectroscopy[7,8] and the spectra have revealed that the Jahn-Teller stabilization of CH_4^+ amounts to more than 1 eV. However, the vibrational assignments provided in Refs. 7 and 8 are entirely different. A major progress was the recording of the rotationally resolved pulsed-field-ionization zero-kinetic-energy photoelectron (PFI-ZEKE-PE) spectrum of CH_4,[9] which was followed by a study of partially and the fully deuterated isotopomers.[10] Although the vibrational structure of CH_4^+ and its isotopomers at low energies could be understood qualitatively with the help of a one-dimensional model for pseudorotation, the spectral structures could only be assigned in the lowest vibronic level of $CH_2D_2^+$ which could be analyzed with an asymmetric rigid rotor Hamiltonian.[11] This analysis established that the isolated

[a]Present address: Department of Biomedical Engineering, Emory University, Atlanta, GA 30322.

$CH_2D_2^+$ cation possesses a C_{2v} equilibrium structure. The model was, however, incapable of reflecting the full symmetry of the problem because of its reduced dimensionality and, therefore, neither the vibronic nor the rovibronic symmetries could be predicted correctly. Moreover, the model did not incorporate the effects of the geometric phase and has underestimated the size of the tunneling splittings.

Theoretically, a C_{2v} equilibrium structure has first been predicted by Meyer[12] from *ab initio* configuration interaction calculations, whereas earlier articles had reported a D_{2d} or C_{3v} minimum energy structure.[13,14] The distortion from the tetrahedral to the C_{2v} geometry leads to 12 equivalent minima which can be separated in two enantiomeric sets. Detailed investigations of the potential energy surface[15,16] revealed that the barriers between the six minima within one set are low and that CH_4^+ undergoes a large-amplitude tunneling motion. The predicted barrier height lies in the range of 350–1050 cm^{-1} (Refs. 15–17) but is strongly dependent on the level of the *ab initio* calculations and/or the method used to represent the potential energy surface. The large-amplitude motion can be understood as a cyclic exchange of three hydrogen atoms via a saddle point of C_s symmetry.[15] Apart from the attempts of Takeshita,[18] Marinelli and Roche,[19] Reeves and Davidson,[20] and Signorell and Sommavilla,[21] no calculations of the rovibronic structure of CH_4^+ have been reported.

The Jahn-Teller effect of an orbitally threefold degenerate state interacting with vibrations of symmetries e and f_2, denoted $T\otimes(e\oplus t_2)$, has been studied theoretically. Öpik and Pryce[22] were the first to study the number and types of possible minima on the lowest potential energy surface and found that the minima are either trigonal or tetragonal, i.e., of C_{3v} or D_{2d} symmetry for a tetrahedral molecule. Bersuker and Polinger[23] have subsequently discovered that the inclusion of quadratic vibronic coupling terms allows points of C_{2v} symmetry to become minima and have studied the tunneling splittings associated with this situation. Although the $T\otimes(e\oplus t_2)$ problem is very common in crystals, it could not be studied in detail so far, because high-resolution gas-phase spectroscopic data were not available or not assigned. This is in contrast to the $E\otimes e$ JT problem which is now well understood in several molecular systems.[24]

Large-amplitude motions are of fundamental importance for the understanding of molecular structure and dynamics. The JT effect is often associated with a particularly interesting category of large-amplitude motions which are referred to as "pseudorotations." This type of motion connects equivalent minima of the potential energy surfaces with each other and takes place when the barriers between them are low enough. This situation applies, for instance, to the ground states of Li_3 and Na_3 which possess three equivalent minima and have been characterized in detail by high-resolution spectroscopy.[25–27] Several theoretical methods have been developed to analyze the tunneling-rotation structure in such systems. The most accurate treatment is achieved by a full variational calculation including all degrees of freedom[28] which predicted the tunneling-rotation spectrum of Na_3 in excellent agreement with the experiment. Several effective Hamiltonian models have been developed for the alkali trimers. Ohashi *et al.* have derived an effective rotation-pseudorotation Hamiltonian[29] that includes all operators allowed by symmetry and have obtained a quantitative agreement with the experimental data. Mayer and Cederbaum[30] have developed a general formalism to calculate rotational structures of vibronically coupled systems. Its first step consists of solving the vibronic problem in a product basis of diabatic electronic and harmonic oscillator basis functions. In a second step, an effective rotational Hamiltonian is constructed for which all parameters can be calculated from the vibronic eigenvectors. To our knowledge, the combined treatment of rotation and pseudorotation in tetrahedral symmetry has not been considered so far.

The present article is organized as follows. The next section describes the experimental measurement and assignment procedures. Section III is devoted to the derivation of the tunneling matrix and the effective tunneling-rotation Hamiltonian. Section IV presents the PFI-ZEKE spectra of $^{12}CH_4$, $^{13}CH_4$, and $^{12}CD_4$, their assignment, and the simulation of the spectra with the tunneling-rotation Hamiltonian. In Sec. V the results of the analysis are discussed and compared to *ab initio* data and earlier results.

II. EXPERIMENT

The photoion/photoelectron spectrometer and the VUV light source used in the present experiments have been described previously.[31] Methane (Pangas, 99.995% purity), $^{13}CH_4$ [Cambridge isotope laboratories (CIL), 98% chemical purity, 98% isotopic enrichment], and CD_4 (CIL, 98% chemical purity, 98% isotopic enrichment) were introduced into the spectrometer by means of a pulsed, skimmed supersonic expansion. The valve was operated at a repetition rate of 10 Hz and a stagnation pressure of 2–3 bars. Expansions of either the pure gas or a mixture with Ar were used. VUV radiation was generated by two-photon resonance-enhanced sum-frequency mixing ($\nu_{VUV}=2\nu_1+\nu_2$) of the output of two Nd:YAG (yttrium aluminum garnet) pumped dye lasers in Xe using the $(5p)^5 6p[1/2]_0 \leftarrow (5p)^6\ ^1S_0$ two-photon resonance at $2\tilde{\nu}_1=80\,118.964\ cm^{-1}$. The VUV radiation was separated from the fundamental beams in a vacuum monochromator using a toroidal dispersion grating which also recollimated the diverging VUV beam and redirected it toward a photoexcitation-photoionization chamber where it intersected the molecular beam at right angles. IR radiation around 3000 cm^{-1} (6000 cm^{-1}) was generated by difference-frequency mixing in a $KTiOAsO_4$ or KTA ($KTiOPO_4$ or KTP) crystal.[32,33] A KTA (KTP) crystal of dimensions of $5\times5\times15\ mm^3$ ($5\times5\times10\ mm^3$) was used. The 532 nm (1064 nm) output of the Nd:YAG laser and the 630–640 nm (645–655 nm) output of a tunable dye laser were overlapped by means of a dichroic mirror and collimated to a beam of waist 1.5 mm before being sent into the crystal. Phase matching was achieved by adjusting the angle between the laser beams and the crystal axis. The two input beams were aligned so that they crossed in the center of the crystal with a small angle between them. This alignment allowed a simple separation of the different beams after the crystal and avoided the use of filters. Pulse energies of up to 1 mJ were

obtained around 3.3 μm (1.6 μm) using pulse energies of 10 mJ at 630 nm (650 nm) and 15 mJ at 532 nm (1064 nm). The IR beam was then sent into the photoexcitation chamber using gold-coated mirrors and counterpropagated against the VUV beam. The IR pulse was timed to preceed the VUV pulse by ≈10 ns. The IR frequency was calibrated by comparing the measured line positions of the ν_3 and $2\nu_3$ bands of CH_4 with literature values.[34] Calibration of the visible radiation was achieved by recording optogalvanic spectra of neon and comparing the observed wave numbers to the tables given in Ref. 35. The VUV wave number was determined by building the sum of the two-photon resonance wave number and the wave number of the second laser which was also determined by recording optogalvanic spectra of neon.

PFI-ZEKE photoelectron spectra were recorded by monitoring the pulsed electric field ionization of high Rydberg states located immediately below the ionization thresholds as a function of the laser wave number. A positive pulsed electric field of less than 1 V/cm and of 1 μs duration was applied 1 μs after photoexcitation and was immediately followed by a negative pulsed electric field of comparable amplitude. The first (discrimination) pulse served the purpose of removing prompt electrons and of ionizing the highest Rydberg states. The PFI-ZEKE spectra were obtained by recording the field-ionization yield of the second pulse.

The absolute positions of the ionic levels above the neutral ground state were determined from the measured wave numbers of the PFI-ZEKE lines after a correction was made to account for the shifts of the ionization thresholds induced by the electric fields according to the procedure described in Ref. 36.

Four different experiments were performed. First, single-photon VUV PFI-ZEKE photoelectron spectra were recorded by monitoring the pulsed-field-ionization electron signal as a function of the VUV wave number for the species CH_4, $^{13}CH_4$, and CD_4. Second, IR spectra of the ν_3 and $2\nu_3$ bands were recorded by setting the VUV wave number just below the adiabatic ionization energy and recording the ion signal as a function of the IR wave number. Third, IR+VUV resonance-enhanced two-photon spectra of CH_4 were recorded by holding the IR wave number fixed on a selected rovibrational transition of the asymmetric stretch fundamental (ν_3) or its first overtone ($2\nu_3$) and tuning the VUV laser. Finally, "ZEKE dip" measurements were performed for CH_4 in which the VUV frequency was held at the position of a given line in the single-photon PFI-ZEKE spectrum, and the depletion of the photoelectron signal was monitored at the three IR frequencies corresponding to the $R(0)$, $R(1)$, and $R(2)$ lines of the ν_3 band. In these measurements, pulse energies of ≈200 μJ (beam waist ≈2 mm) were sufficient to entirely saturate the infrared transitions. Depletions of up to 50% were observed whenever the IR and VUV transitions had a common lower level.

The rotationally resolved IR spectra of CH_4 and $^{13}CH_4$ around 6000 cm^{-1} are shown in Figs. 1(a) and 1(b), respectively. The spectra correspond to the transition from the neutral ground state to the $v_3=2$ vibrational level. The observed transitions are easily assigned to $P(2)$, $P(1)$, an unresolved Q branch, $R(0)$, $R(1)$, and $R(2)$, and the measured wave numbers correspond well with the literature values given in Ref. 34. These spectra indicate that only the lowest state of each nuclear spin symmetry ($J=0$ corresponding to nuclear spin symmetry A_1, $J=1$ to F_2, and $J=2$ to E) is populated significantly in the supersonic beam, which corresponds to a rotational temperature of less than 7 K.

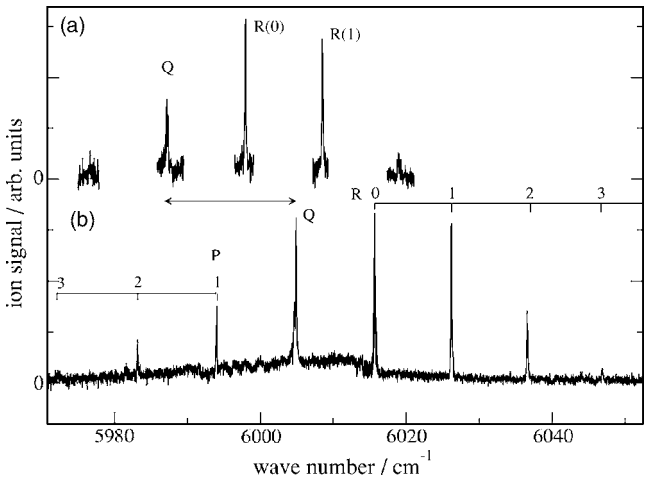

FIG. 1. Spectra of jet-cooled $^{13}CH_4$ [trace (a)] and CH_4 [trace (b)] in the region of the $2\nu_3$ overtone transition recorded by monitoring, as a function of the IR wave number, the ionization of the excited vibrational level with VUV radiation. The transitions are labeled according to the associated changes in rotational angular momentum P ($\Delta J=-1$), Q ($\Delta J=0$), R ($\Delta J=+1$) and the rotational angular momentum quantum number of the initial level. The transitions of $^{13}CH_4$ are redshifted by 17.7 cm^{-1} compared to the transitions of CH_4.

III. THEORY

A. The vibronic problem

A threefold degenerate electronic state of a polyatomic molecule in its tetrahedral reference geometry is subject to vibronic coupling with vibrational modes of e and f_2 symmetries and the corresponding Hamiltonian can be expressed as[23]

$$\hat{H}_{\mathrm{JT}} = \sum_{\Gamma\gamma} -\frac{\hbar^2}{2\mu_\Gamma}\frac{\partial^2}{\partial Q_{\Gamma\gamma}^2}\mathbf{C}_\alpha + \mathbf{U}(Q), \tag{1}$$

with

$$\begin{aligned}\mathbf{U}(Q) = \sum_{\Gamma\gamma}\left(\frac{1}{2}G_\Gamma Q_{\Gamma\gamma}^2\mathbf{C}_\alpha + V_\Gamma Q_{\Gamma\gamma}\mathbf{C}_{\Gamma\gamma}\right) \\ + W\left[Q_\xi\left(-\frac{1}{2}Q_\theta + \frac{\sqrt{3}}{2}Q_\epsilon\right)\mathbf{C}_\xi\right. \\ \left. + Q_\eta\left(-\frac{1}{2}Q_\theta - \frac{\sqrt{3}}{2}Q_\epsilon\right)\mathbf{C}_\eta + Q_\xi Q_\theta \mathbf{C}_\zeta\right] \\ \text{with } \gamma \in \Gamma,\ \Gamma = e, f_2. \end{aligned} \tag{2}$$

$\gamma=\theta,\epsilon$, and ξ,η,ζ denote the components of the irreducible representations e and f_2, respectively, with the transformation properties $\theta\sim 2z^2-x^2-y^2$, $\epsilon\sim\sqrt{3}(x^2-y^2)$, $\xi\sim yz$, $\eta\sim xz$, $\zeta\sim xy$, where x,y,z are the Cartesian coordinates. V_Γ stands for the linear vibronic coupling constants, G_Γ for the sum of quadratic vibronic coupling constants and harmonic

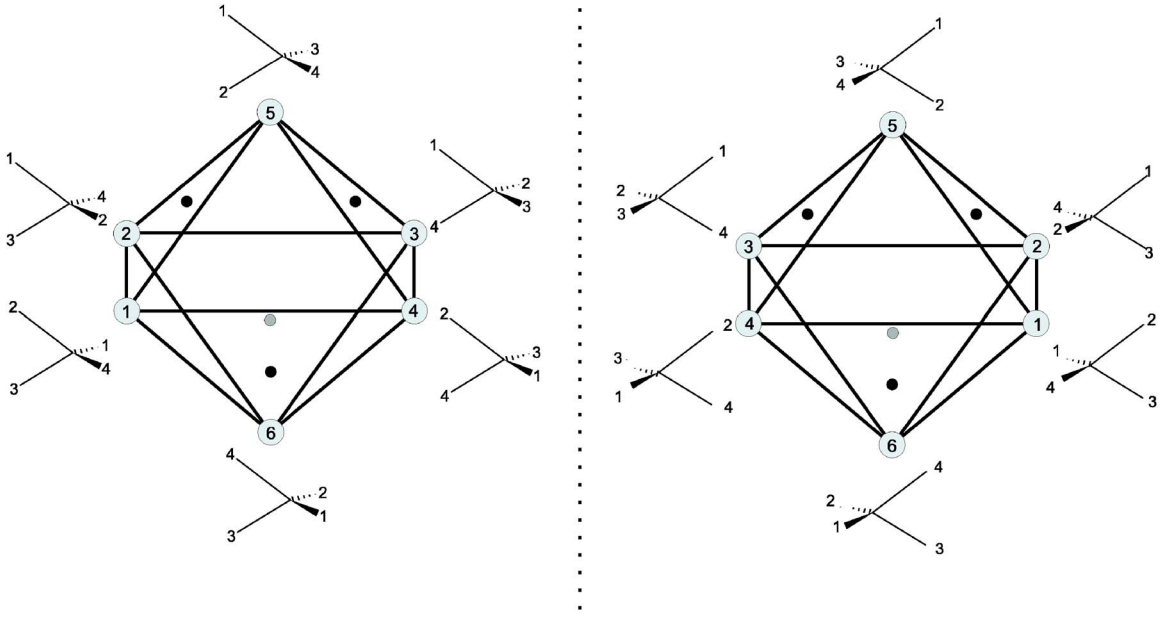

FIG. 2. Topological representation of the connectivity of the 12 equivalent minimum energy structures of C_{2v} symmetry of CH_4^+. The vertices correspond to the C_{2v} minimum energy geometries and the edges to the equivalent pseudorotation-tunneling paths connecting the minima via the low-lying C_s transition states. The dotted line represents the barrier for stereomutation separating each minimum structure from its enantiomer. Four faces of the octahedron correspond to a C_{3v} geometry with a degenerate ground state (marked with a dot) and the other four to a C_{3v} geometry with a nondegenerate ground state (adapted from Ref. 15).

frequencies, and W for the bilinear vibronic coupling constants between modes of symmetries e and f_2 and μ_Γ for the reduced mass corresponding to the $\Gamma = e$ and f_2 modes. The matrices $\mathbf{C}_{\Gamma\gamma}$ of Clebsch-Gordan coefficients defined in the space $|\xi\rangle, |\eta\rangle, |\zeta\rangle$ of functions of the electronic triplet in its reference geometry are given by

$$\mathbf{C}_\alpha = \begin{pmatrix} 1 & 0 & 0 \\ 0 & 1 & 0 \\ 0 & 0 & 1 \end{pmatrix}, \quad \mathbf{C}_\theta = \begin{pmatrix} 1/2 & 0 & 0 \\ 0 & 1/2 & 0 \\ 0 & 0 & -1 \end{pmatrix},$$

$$\mathbf{C}_\epsilon = \begin{pmatrix} -\sqrt{3}/2 & 0 & 0 \\ 0 & \sqrt{3}/2 & 0 \\ 0 & 0 & 0 \end{pmatrix},$$

$$\mathbf{C}_\xi = \begin{pmatrix} 0 & 0 & 0 \\ 0 & 0 & -1 \\ 0 & -1 & 0 \end{pmatrix}, \tag{3}$$

$$\mathbf{C}_\eta = \begin{pmatrix} 0 & 0 & -1 \\ 0 & 0 & 0 \\ -1 & 0 & 0 \end{pmatrix}, \quad \mathbf{C}_\zeta = \begin{pmatrix} 0 & -1 & 0 \\ -1 & 0 & 0 \\ 0 & 0 & 0 \end{pmatrix}.$$

In Hamiltonian (1), only the most important terms have been included, i.e., those that can modify the composition of the electronic eigenfunctions of the potential term $\mathbf{U}(Q)$, which will be used in setting up the tunneling matrices.

The adiabatic potential $E(Q)$ with the corresponding adiabatic electronic wave functions $|a(Q)\rangle$ is defined by the eigenvalue equation

$$\mathbf{U}(Q)|a(Q)\rangle = E(Q)|a(Q)\rangle, \tag{4}$$

and its extremal points have been determined in Refs. 22 and 23. In the absence of quadratic coupling, the distortion of a tetrahedral molecule leads to minima of either C_{3v} or D_{2d} symmetry, whereas the points of C_{2v} symmetry are always saddle points on the lowest adiabatic potential surface.[22] If quadratic coupling is included, the points of C_{2v} symmetry can become minima.[23]

B. The potential energy surface of the methane cation

The most detailed study of the potential energy surfaces of CH_4^+ have been performed by Paddon-Row *et al.*[15] and Frey and Davidson[16] who agree on the essential properties of the potential energy surface, especially the C_{2v} geometry of the minimum energy structure. More recently, the energies of several stationary points have been recalculated at a higher level of theory,[17] and these results are in good agreement with those of Ref. 16. The tetrahedral configuration of CH_4^+ corresponds to a triply degenerate conical intersection that lies approximately 12 000 cm^{-1} above the minima of C_{2v} geometry. A distortion along the modes of symmetry f_2 (ν_3 asymmetric stretch and ν_4 bending) leads to two different structures of C_{3v} geometry that correspond to second-order saddle points on the lowest adiabatic surface. One of them has three equal C–H bonds that are shorter than the fourth C–H bond. This structure has a nondegenerate electronic ground state and a doubly degenerate first excited state. The other C_{3v} structure has three equal C–H bonds that are longer than the fourth and a doubly degenerate electronic ground state. A distortion along the mode of symmetry e (ν_2, bending) leads to a D_{2d} structure that is also a second-order saddle

TABLE I. Correlation table of the rovibronic symmetries from the $T_d(M)$ to the S_4^* molecular symmetry group including nuclear spin-statistical weights for CH_4^+.

$T_d(M)$	S_4^*
$A_1(5)$	$A_1^+(0)\oplus A_2^-(5)$
$A_2(5)$	$A_2^+(5)\oplus A_1^-(0)$
$E(2)$	$E^+(1)\oplus E^-(1)$
$F_1(3)$	$F_1^+(3)\oplus F_2^-(0)$
$F_2(3)$	$F_2^+(0)\oplus F_1^-(3)$

point on the lowest sheet of the potential energy surface. This structure has a nondegenerate ground state and a doubly degenerate first excited state. The minima of C_{2v} geometry result from a distortion along ν_2, ν_3, and ν_4. Two sets of first-order saddle points have also been located and possess a C_s structure. The first lies approximately 1050 cm^{-1} and the second about 5400 cm^{-1} above the minima corresponding to the C_{2v} structure.[15] The number of different possible arrangements of the four hydrogen atoms is equal to the ratio between the order of the complete nuclear permutation-inversion group of CH_4^+ (G_{48} or S_4^*) and the order of the point group of the considered structure. Thus, the tetrahedral geometry allows for $O(G_{48})/O(T_d)=2$ structures that are enantiomers of each other. In C_{3v} geometry there are 8 equivalent structures, 6 in D_{2d}, 12 in C_{2v}, and 24 in C_s.

The 12 equivalent C_{2v} minima of CH_4^+ can be subdivided into two enantiomeric sets of six structures that differ in the numbering of the identical H atoms, as depicted in Fig. 2. The two sets of 12 low-lying first-order saddle points of C_s symmetry correspond to the transition states for the interconversions of minimum energy structures within each set and lie in the middle of the lines connecting the C_{2v} minima, whereas the higher-lying saddle points correspond to the transition state of the inversion of a C_{2v} structure into its enantiomeric structure. The former process corresponds to a cyclic exchange of three hydrogen atoms and repeated cyclic exchanges are referred to as pseudorotation. The latter process corresponds to the stereomutation of CH_4^+ (Refs. 37 and 38). At the resolution of up to 0.3 cm^{-1} of the present experiments, one can expect to observe tunneling splittings resulting from the pseudorotational motion in the ground state. The barrier of about 5400 cm^{-1} for stereomutation is too high for the inversion splittings to be observable. The order of the molecular symmetry group can therefore be reduced by removing all operations that interconvert enantiomers. G_{48} (see Ref. 39) and S_4^* (see Ref. 40) contain operations of the types E, (123), (12)(34), (12), (1234), E^*, $(123)^*$, $(12)\times(34)^*$, $(12)^*$, and $(1234)^*$. The operations E^* and those of the types (12), $(123)^*$, (1234), and $(12)(34)^*$ interconvert enantiomers and are not feasible. The resulting group is $T_d(M)$ and is the adequate molecular symmetry group to describe the rovibronic levels of CH_4^+ and CD_4^+ as long as the inversion splittings are not resolved.

The correlation of the rovibronic symmetry labels in the $T_d(M)$ and S_4^* groups including spin-statistical weights for CH_4^+ and CD_4^+ are given in Tables I and II, respectively. At sufficient resolution, the stereomutation of CH_4^+ could be observed as a splitting of the levels of rovibronic symmetry E because both parity components of this symmetry have a nonzero spin-statistical weight. The observation of stereomutation is much easier in CH_4^+ than in CH_4 because the latter has a stereomutation barrier that is comparable to the C–H bond dissociation energy, i.e., about 36 000 cm^{-1}.[37] Because we have not observed tunneling splittings associated with the stereomutation, the following arguments will be restricted to one enantiomeric set of six C_{2v} structures and will be developed using the $T_d(M)$ group. The derivation of the correlation presented in Table I is essential for the understanding of the spectra of CH_4^+ but does not correspond to the correlation given in Ref. 20, with the important consequence that the rotationless ground state of CH_4^+ has a nonzero spin-statistical weight.

C. The tunneling problem

In the light of the *ab initio* results summarized in Sec. III B, the lowest band of the PFI-ZEKE photoelectron spectrum of CH_4 is expected to reveal the effects of a tunneling motion. Tunneling is most simply treated in a matrix representation using basis states that are strongly localized in the vicinity of the minimum energy structures.[41] The basis states used in the present analysis are defined as follows:

$$\phi_n = |n\rangle|\chi_n\rangle, \tag{5}$$

where $|n\rangle=|a(Q_n)\rangle$ is the adiabatic electronic function in the nth potential well and $|\chi_n\rangle$ represents the ground state vibrational function (a product of 9 harmonic oscillator functions) of the molecule in the nth potential well.

The adiabatic electronic functions at the geometries of the six C_{2v} minima $|n\rangle=\frac{1}{\sqrt{2}}(|\xi\rangle+|\eta\rangle)$, $\frac{1}{\sqrt{2}}(|\xi\rangle+|\zeta\rangle)$, $\frac{1}{\sqrt{2}}(-|\xi\rangle+|\eta\rangle)$, $\frac{1}{\sqrt{2}}(-|\xi\rangle+|\zeta\rangle)$, $\frac{1}{\sqrt{2}}(|\eta\rangle-|\zeta\rangle)$, and $\frac{1}{\sqrt{2}}(|\eta\rangle+|\zeta\rangle)$ are obtained by diagonalizing the potential term $\mathbf{U}(Q)$ for CH_4^+ that was derived in Ref. 16.

These eigenfunctions have a general validity for C_{2v} minima resulting from a $T\otimes(e\oplus t_2)$ Jahn-Teller effect and are indeed equivalent to those obtained by Bersuker and Polinger.[23] The construction of the tunneling matrix is significantly simplified by the permutational symmetry of CH_4^+ and CD_4^+ because all 6 C_{2v} minima are equivalent and so are the 12 C_s saddle points connecting the minima. The elements of the matrix are defined by $H_{ij}=\langle i|j\rangle\langle\chi_i|\hat{H}_{\text{vib}}|\chi_j\rangle$ and $S_{ij}=\langle i|j\rangle\langle\chi_i|\chi_j\rangle$, where $\hat{H}_{\text{vib}}$ is the vibrational Hamiltonian for the lowest potential energy surface. The resulting generalized eigenvalue problem takes the form of a determinantal equation[1]

TABLE II. Same as Table I but with nuclear spin-statistical weights for CD_4^+.

$T_d(M)$	S_4^*
$A_1(15)$	$A_1^+(15)\oplus A_2^-(0)$
$A_2(15)$	$A_2^+(0)\oplus A_1^-(15)$
$E(12)$	$E^+(6)\oplus E^-(6)$
$F_1(18)$	$F_1^+(3)\oplus F_2^-(15)$
$F_2(18)$	$F_2^+(15)\oplus F_1^-(3)$

$$\begin{vmatrix} H_{11}-E & H_{12}-S_{12}E & 0 & -(H_{12}-S_{12}E) & H_{12}-S_{12}E & H_{12}-S_{12}E \\ H_{12}-S_{12}E & H_{11}-E & -(H_{12}-S_{12}E) & 0 & -(H_{12}-S_{12}E) & H_{12}-S_{12}E \\ 0 & -(H_{12}-S_{12}E) & H_{11}-E & H_{12}-S_{12}E & H_{12}-S_{12}E & H_{12}-S_{12}E \\ -(H_{12}-S_{12}E) & 0 & H_{12}-S_{12}E & H_{11}-E & -(H_{12}-S_{12}E) & H_{12}-S_{12}E \\ H_{12}-S_{12}E & -(H_{12}-S_{12}E) & H_{12}-S_{12}E & -(H_{12}-S_{12}E) & H_{11}-E & 0 \\ H_{12}-S_{12}E & H_{12}-S_{12}E & H_{12}-S_{12}E & H_{12}-S_{12}E & 0 & H_{11}-E \end{vmatrix} = 0, \quad (6)$$

where $H_{11}=\langle\chi_1|\hat{H}|\chi_1\rangle$, $S_{11}=\langle\chi_1|\chi_1\rangle$, $H_{12}=1/2\langle\chi_1|\hat{H}|\chi_2\rangle$, and $S_{12}=1/2\langle\chi_1|\chi_2\rangle$.

The solutions of the determinantal equation [Eq. (6)] are two sets of triply degenerate levels (F_2 and F_1),

$$E_{F_2}=\frac{H_{11}+2H_{12}}{1+2S_{12}} \quad \text{and} \quad E_{F_1}=\frac{H_{11}-2H_{12}}{1-2S_{12}}, \quad (7)$$

with associated eigenvectors

$$\mathbf{U}=\frac{1}{2}\begin{pmatrix} 1 & 0 & -1 & -1 & 0 & 1 \\ 0 & 1 & -1 & 0 & 1 & -1 \\ 1 & 0 & 1 & -1 & 0 & -1 \\ 0 & 1 & 1 & 0 & 1 & 1 \\ 1 & -1 & 0 & 1 & 1 & 0 \\ 1 & 1 & 0 & 1 & -1 & 0 \end{pmatrix}, \quad (8)$$

where the first three columns are the eigenvectors of vibronic symmetry F_2 and the last three columns those of symmetry F_1. The tunneling integral H_{12} is negative which results in the F_2 level being the ground state. The value of the overlap integral S_{ij} has no influence on the nature of the eigenvectors but it affects the value of the tunneling splitting $\delta=|E_{F_2}-E_{F_1}|$.

This tunneling model can also be used to predict the nature of the ground state in the case where the minimum energy structures have a different symmetry. If the minimum energy structure is of D_{2d} geometry and inversion is still neglected, only three minima must be considered. These structures correspond to a distortion along the e mode only and the corresponding Clebsch-Gordan matrices are diagonal. Consequently, the adiabatic wave functions corresponding to the lowest energy in the three minima are simply equal to the diabatic basis functions $|\xi\rangle,|\eta\rangle,|\zeta\rangle$. Because these functions are orthogonal to each other, there is no tunneling and the lowest vibronic level has the vibronic symmetry F_2. This conclusion has also been reached in the analysis of the $T\otimes e$ JT effect in Ref. 42. If the minimum energy structure has C_{3v} geometry, which corresponds to the $T\otimes t_2$ JT effect, four minima arise with the following adiabatic electronic wave functions: $1/\sqrt{3}(|\xi\rangle+|\eta\rangle+|\zeta\rangle)$, $1/\sqrt{3}(|\xi\rangle-|\eta\rangle-|\zeta\rangle)$, $1/\sqrt{3}(-|\xi\rangle+|\eta\rangle-|\zeta\rangle)$, and $1/\sqrt{3}(-|\xi\rangle-|\eta\rangle+|\zeta\rangle)$. Assuming a negative tunneling matrix element, tunneling splits this fourfold degenerate ground state into a threefold degenerate state of symmetry F_2 lying below a nondegenerate state of A_1 symmetry. This result has also been obtained in Ref. 43, where the level ordering has been shown to derive from a geometric phase. A common feature of all three cases is that the lowest level has vibronic symmetry F_2, i.e., the same symmetry as the electronic state in the undistorted geometry. This situation is characteristic of most Jahn-Teller problems, although exceptions have been found for large values of the quadratic coupling constants.[44,45]

The symmetry of the tunneling states corresponding to a given minimum energy geometry can also be predicted from group theoretical arguments. First, the electronic symmetry of the ground electronic state of the molecule is determined in the point group corresponding to the minimum energy structure. Then, the corresponding irreducible representation is correlated to the molecular symmetry group of the molecule. This procedure provides the symmetry labels for the tunneling states in the molecular symmetry group directly. A minimum energy structure of C_{2v} symmetry in CH_4^+ has a ground state of electronic symmetry B_2 (according to the conventions in Ref. 10). The correlation between C_{2v} and $T_d(M)$, listed in Table III, gives $F_1\oplus F_2$ for the rovibronic symmetries of the tunneling states, which corresponds to the result of the tunneling calculation given above. Similarly, a D_{2d} structure of CH_4^+ possesses a B_2 ground state which correlates with F_2 in $T_d(M)$, and a C_{3v} structure has an A_1 ground state which correlates with $F_2\oplus A_1$ in $T_d(M)$. The method can also be applied to distortions that do not result from a degeneracy on the ground state surface but occur, e.g., in molecules subject to a Pseudo-Jahn-Teller (PJT) effect.[24] For example, we consider a tetrahedral molecule with an electronic ground state of symmetry A_1 that is distorted by a PJT effect. The electronic symmetry in C_{2v} geometry can only be A_1, as can be derived from Table III. If a tunneling process analogous to the one discussed above were observable, the correlation to $T_d(M)$ would predict tunneling states of symmetries $A_1\oplus E\oplus F_2$, a result that was also obtained from tunneling calculations excluding the geometric phase.[1] The absence of electronic degeneracy in the ground state of the tetrahedral geometry thus leads to a profoundly altered tunneling structure.

TABLE III. Reverse correlation table of irreducible representations of the C_{2v} point group to the $T_d(M)$ molecular symmetry group.

C_{2v}	$T_d(M)$
A_1	$A_1\oplus E\oplus F_2$
A_2	$A_2\oplus E\oplus F_1$
B_1	$F_1\oplus F_2$
B_2	$F_1\oplus F_2$

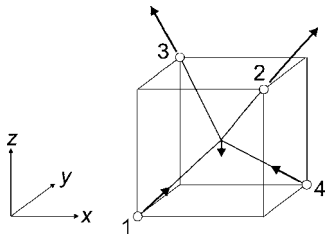

FIG. 3. Global axis system defined with respect to the tetrahedral reference geometry of CH_4^+. The rotational basis functions $|JK\rangle$ used in the tunneling-rotation treatment are defined in this axis system.

D. The rovibronic problem

To treat the rotational structure in the lowest tunneling states, it is convenient to use a set of rotational basis functions defined in an axis system that is common to all distorted structures. This axis system is defined with respect to the undistorted molecule and is represented in Fig. 3. The derivation of the rotational Hamiltonian can be divided into two steps. First, the molecule is taken in its tetrahedral reference configuration and is distorted along one of the axes to a C_{2v} minimum energy structure. The type of distortion is indicated in Table IV by two numbers in square brackets designating the hydrogen atoms that are moved away from the carbon atom and by the axis along which the C atom is displaced. The distortion depicted by arrows in Fig. 4 is thus denoted [23]/−z. Along each axis there are two possible distortions, so that a total of six distorted structures result. Second, the axis system is rotated such that it coincides with the principal axis system of the distorted structure, as illustrated in Fig. 4, for the structure labeled 1 on the right-hand side of Fig. 2. In this axis system, the rotational Hamiltonian takes the simple form

$$\frac{\hat{H}_{\mathrm{rot}}^{(1)}}{hc} = B\hat{J}_{x'}^2 + C\hat{J}_{y'}^2 + A\hat{J}_{z'}^2, \tag{9}$$

where the superscript in parentheses designates the minimum energy structure in Fig. 2. Inserting the expressions for the rotational operators $\hat{J}_{x'}, \hat{J}_{y'}, \hat{J}_{z'}$ in terms of the operators defined in the global axis system, one obtains the expressions given in Table IV for the rotational Hamiltonian in each minimum.

The basis used to solve the rovibronic problem consists of the direct product of the basis states of the pure tunneling problem and symmetric top eigenfunctions $|JK\rangle$,

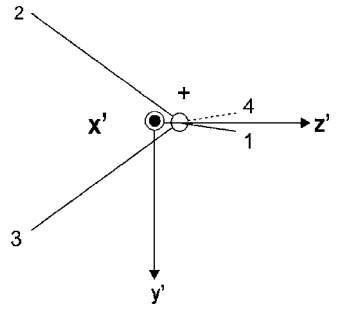

FIG. 4. Principal axis system used for the minimum energy structure labeled 1 on the right-hand side of Fig. 2.

$$\phi_{n,JK} = |n\rangle|\chi_n\rangle|JK\rangle, \tag{10}$$

where J is the rotational angular momentum quantum number and K the quantum number for its projection on the z axis.

The tunneling-rotation Hamiltonian is defined as

$$\hat{H} = \hat{H}_{\mathrm{vib}} + \hat{H}_{\mathrm{rot}}. \tag{11}$$

Its matrix representation in the basis $\phi_{n,JK}$ possesses the following elements:

$$\begin{aligned} H_{ij,JKJ'K'} &= \langle i|j\rangle(\langle\chi_i|\hat{H}_{\mathrm{vib}}|\chi_j\rangle\langle JK|J'K'\rangle \\ &\quad + \langle\chi_i|\chi_j\rangle\langle JK|\hat{H}_{\mathrm{rot}}|J'K'\rangle) \\ &= \langle i|j\rangle(\langle\chi_i|\hat{H}_{\mathrm{vib}}|\chi_j\rangle\delta_{JJ'}\delta_{KK'} + \delta_{ij}\langle JK|\hat{H}_{\mathrm{rot}}|J'K'\rangle) \\ &= \begin{cases} \langle JK|\hat{H}_{\mathrm{rot}}^{(i)}|J'K'\rangle & \text{for } i=j \\ \langle i|j\rangle 2\sigma\delta_{JJ'}\delta_{KK'} & \text{for } i\neq j, \end{cases} \end{aligned} \tag{12}$$

where we have defined $\sigma = 1/2\langle\chi_i|\hat{H}|\chi_j\rangle$ and assumed that $\langle\chi_i|\chi_j\rangle = \delta_{ij}$.

The diagonalization of this matrix provides the tunneling-rotation eigenvalues and eigenvectors. For $J=0$ we obtain two eigenvectors of rovibronic symmetries F_2 and F_1 with the eigenvalues $E_{F_2}=2\sigma$ and $E_{F_1}=-2\sigma$, respectively. This result is indeed equivalent to Eq. (7) with $H_{11}=S_{12}=0$, $H_{12}=\sigma<0$ and, in the limit of zero overlap ($\langle\chi_i|\chi_j\rangle=0$, for $i\neq j$), establishes the relation $\delta=4|\sigma|$ between the tunneling matrix element σ and the tunneling splitting δ of the $J=0$ level.

TABLE IV. Localized asymmetric top Hamiltonian for each minimum defined in the global axis system of Fig. 3. The second column indicates the type of distortion as discussed in the text.

Min.	Type of distortion	Asymmetric top Hamiltonian
1	[23]/−z	$\hat{H}_{\mathrm{rot}}^{(1)}/hc = \frac{1}{2}(C+B)(\hat{J}_x^2+\hat{J}_y^2) + \frac{1}{2}(B-C)(\hat{J}_x\hat{J}_y+\hat{J}_y\hat{J}_x) + A\hat{J}_z^2$
2	[13]/−y	$\hat{H}_{\mathrm{rot}}^{(2)}/hc = \frac{1}{2}(C+B)(\hat{J}_z^2+\hat{J}_x^2) + \frac{1}{2}(B-C)(\hat{J}_z\hat{J}_x+\hat{J}_x\hat{J}_z) + A\hat{J}_y^2$
3	[14]/z	$\hat{H}_{\mathrm{rot}}^{(3)}/hc = \frac{1}{2}(C+B)(\hat{J}_x^2+\hat{J}_y^2) - \frac{1}{2}(B-C)(\hat{J}_x\hat{J}_y+\hat{J}_y\hat{J}_x) + A\hat{J}_z^2$
4	[24]/y	$\hat{H}_{\mathrm{rot}}^{(4)}/hc = \frac{1}{2}(C+B)(\hat{J}_z^2+\hat{J}_x^2) - \frac{1}{2}(B-C)(\hat{J}_z\hat{J}_x+\hat{J}_x\hat{J}_z) + A\hat{J}_y^2$
5	[12]/−x	$\hat{H}_{\mathrm{rot}}^{(5)}/hc = \frac{1}{2}(C+B)(\hat{J}_y^2+\hat{J}_z^2) + \frac{1}{2}(B-C)(\hat{J}_y\hat{J}_z+\hat{J}_z\hat{J}_y) + A\hat{J}_x^2$
6	[34]/x	$\hat{H}_{\mathrm{rot}}^{(6)}/hc = \frac{1}{2}(C+B)(\hat{J}_y^2+\hat{J}_z^2) - \frac{1}{2}(B-C)(\hat{J}_y\hat{J}_z+\hat{J}_z\hat{J}_y) + A\hat{J}_x^2$

E. A general effective tunneling-rotation Hamiltonian

The same effective tunneling-rotation Hamiltonian can also be obtained in the basis of the eigenstates of Eq. (6) as

$$\hat{H}_{\mathrm{rve}} = U^T \hat{H}^{\mathrm{rot}} U + \hat{H}_{\mathrm{ve}}, \tag{13}$$

where $\hat{H}^{\mathrm{rot}}$ is a diagonal matrix of rotational operators of the form of Eq. (9) for the six local C_{2v} structures and U is the eigenvector matrix [Eq. (8)] of the determinantal equation [Eq. (6)]. $\hat{H}_{\mathrm{ve}}$ is diagonal with eigenvalues 0 for the lower tunneling component of F_2 symmetry and δ for the upper tunneling component of F_1 symmetry [see Eq. (7)]. Equation (13) was used in the previous article[1] and has the same eigenvalues as the tunneling-rotation matrix defined by Eq. (12). Equation (13) can be used to derive the formal expression

$$\hat{H}_{\mathrm{rve}} = \frac{1}{4}\begin{pmatrix} E\hat{J}^2 - D\hat{J}_y^2 & -(B-C)(\hat{J}_y\hat{J}_z+\hat{J}_z\hat{J}_y) & -(B-C)(\hat{J}_x\hat{J}_y+\hat{J}_y\hat{J}_x) & D(\hat{J}_x^2-\hat{J}_z^2) & (B-C)(\hat{J}_y\hat{J}_z+\hat{J}_z\hat{J}_y) & (B-C)(\hat{J}_x\hat{J}_y+\hat{J}_y\hat{J}_x) \\ & E\hat{J}^2 - D\hat{J}_z^2 & -(B-C)(\hat{J}_z\hat{J}_x+\hat{J}_x\hat{J}_z) & -(B-C)(\hat{J}_y\hat{J}_z+\hat{J}_z\hat{J}_y) & D(-\hat{J}_x^2+\hat{J}_y^2) & -(B-C)(\hat{J}_z\hat{J}_x+\hat{J}_x\hat{J}_z) \\ & & E\hat{J}^2 - D\hat{J}_x^2 & (B-C)(\hat{J}_x\hat{J}_y+\hat{J}_y\hat{J}_x) & -(B-C)(\hat{J}_z\hat{J}_x+\hat{J}_x\hat{J}_z) & D(\hat{J}_y^2-\hat{J}_z^2) \\ & & & E\hat{J}^2 - D\hat{J}_y^2+\delta & (B-C)(\hat{J}_y\hat{J}_z+\hat{J}_z\hat{J}_y) & -(B-C)(\hat{J}_x\hat{J}_y+\hat{J}_y\hat{J}_x) \\ & \text{H.c.} & & & E\hat{J}^2 - D\hat{J}_z^2+\delta & -(B-C)(\hat{J}_z\hat{J}_x+\hat{J}_x\hat{J}_z) \\ & & & & & E\hat{J}^2 - D\hat{J}_x^2+\delta \end{pmatrix}, \tag{14}$$

for the tunneling-rotation Hamiltonian (H.c. means Hermitian conjugate), where the upper 3×3 block on the diagonal corresponds to the vibronic state of symmetry F_2, the lower block to the F_1 vibronic state, $E=2A+B+C$, and $D=2A-B-C$. In order to rationalize the rovibronic coupling terms contained in Hamiltonian (14), we have classified the rotational operators in the $T_d(M)$ group and the result is given in Table V. The diagonal elements in Eq. (14) correspond to the sum of a term of symmetry A_1 and a term of symmetry E. The off-diagonal elements of the diagonal blocks have symmetry F_2. Turning to the off-diagonal blocks, one finds a term of symmetry E on the diagonal and terms of symmetry F_2 on the off-diagonal positions. All angular momentum operators appearing in this Hamiltonian are multiplied by some linear combinations of the asymmetric top rotational constants A,B,C. Since Hamiltonian (13) has been set up in the limit of a strong static distortion, it does not contain electronic and vibrational angular momentum operators and, therefore, the rotational angular momenta are equal to the total angular momenta.

An alternative way of deriving an effective rotational Hamiltonian for a pair of closely spaced vibronic levels of symmetries F_2 and F_1 is by introducing all components and products of components of the total angular momentum operators up to second order that are allowed by symmetry in a 6×6 matrix representing the vibronic basis. Such a Hamiltonian can be set up by assuming that the vibronic problem has been solved and that its eigenvalues and eigenfunctions are available as discussed in Ref. 30. Angular momentum operators that are linear combinations of terms of the form $\hat{J}_\alpha\hat{J}_\beta(\alpha,\beta=x,y,z)$ will be designated collectively by $\hat{J}_\alpha\hat{J}_\beta$ and the terms linear in $\hat{J}$ by $\hat{J}_\alpha$. Total angular momentum operators of the form $\hat{J}_\alpha$ and $\hat{J}_\alpha\hat{J}_\beta$ can couple two vibronic states if the total rovibronic operators are totally symmetric, i.e., if

$$\begin{aligned} &\Gamma_{\Psi_i}\times\Gamma_{\Psi_j}\times\Gamma_{J_\alpha}\supset A_1 \text{ or} \\ &\Gamma_{\Psi_i}\times\Gamma_{\Psi_j}\times\Gamma_{J_\alpha}\times\Gamma_{J_\beta}\supset A_1, \end{aligned} \tag{15}$$

respectively. In Eq. (15) Γ_{Ψ_i} and Γ_{J_α} designate the irreducible representations of the vibronic basis functions and the component of the total angular momentum operator, respectively. The positions of the angular momentum operators in the rovibronic Hamiltonian matrix is defined by the Clebsch-Gordan matrices for the products of irreducible representations of $T_d(M)$.

A comparison of such a general effective Hamiltonian with the one derived in Eq. (14) provides a physical interpretation of our effective Hamiltonian. The totally symmetric

TABLE V. Rotational operators $\hat{H}_{\mathrm{rot}}$ and their irreducible representation Γ_γ in the $T_d(M)$ molecular symmetry group.

$\hat{H}_{\mathrm{rot}}$	Γ_γ
$\hat{J}^2$	A_1
$1/\sqrt{6}(\hat{J}_x^2+\hat{J}_y^2-2\hat{J}_z^2)$	E_θ
$1/\sqrt{2}(\hat{J}_x^2-\hat{J}_y^2)$	E_ϕ
$1/\sqrt{2}(\hat{J}_y\hat{J}_z+\hat{J}_z\hat{J}_y)$	F_{2x}
$1/\sqrt{2}(\hat{J}_x\hat{J}_z+\hat{J}_z\hat{J}_x)$	F_{2y}
$1/\sqrt{2}(\hat{J}_y\hat{J}_x+\hat{J}_x\hat{J}_y)$	F_{2z}
$\hat{J}_x$	F_{1x}
$\hat{J}_y$	F_{1y}
$\hat{J}_z$	F_{1z}

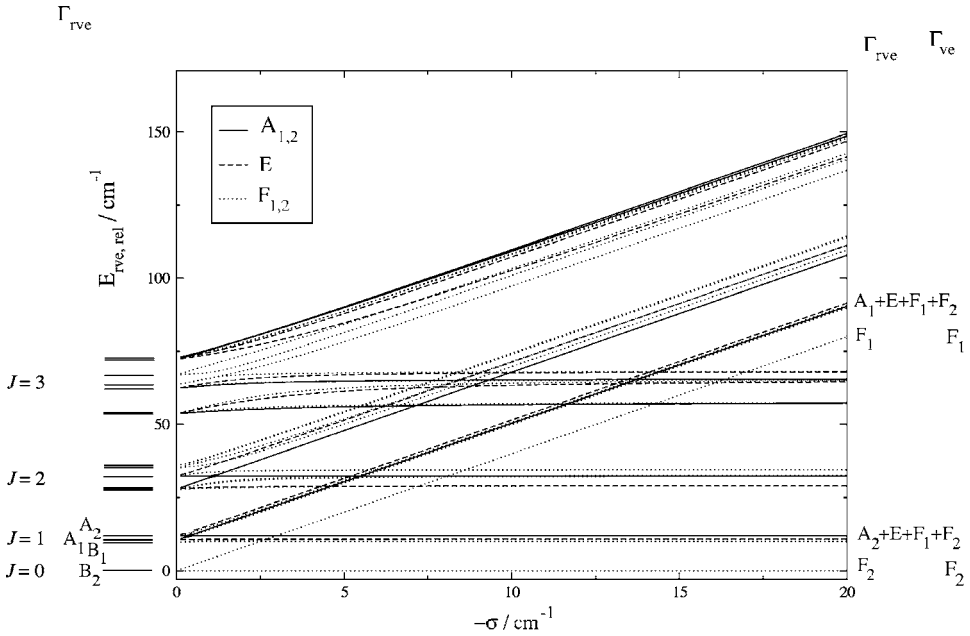

FIG. 5. Correlation diagram of the eigenvalues of tunneling-rotation Hamiltonian (13) as a function of the tunneling integral σ. In the limit $\sigma=0$, all levels are sixfold degenerate and coincide with the pattern of an asymmetric top which is depicted on the left-hand side. Rovibronic symmetries in the C_{2v} point group (left) and $T_d(M)$ molecular symmetry group (right) are assigned to the levels. The vibronic symmetry in the $T_d(M)$ group is indicated on the right-hand side.

term on the diagonal represents the rotational energy of the undistorted molecule and takes the form of a spherical top Hamiltonian with rotational constant $(2A+B+C)/4$. The terms of symmetries E and F_2 in the 3×3 blocks on the diagonal represent the effects of the molecular distortion on the rotation of the molecule. The off-diagonal block contains operators that represent rovibronic coupling between the two vibronic states. From this analysis, we conclude that Hamiltonian (14) contains all allowed operators in the expected positions, with exception of terms of the form $\hat{J}_\alpha$. These terms represent Coriolis interactions between the rotational and the electronic and vibrational angular momenta. These interactions are absent in Hamiltonians (13) and (14) because these do not contain any electronic or vibrational angular momenta. An electronic angular momentum is in principle present because the ground state of CH_4^+ is triply degenerate in the tetrahedral configuration and vibrational angular momentum results from the pseudorotational motion. Although the effects of these angular momenta have not been quantified for CH_4^+, it has been shown that electronic and vibrational angular momenta are quenched by strong Jahn-Teller distortions.[46] Therefore, Coriolis interactions are not expected to dominate the level structure and the approximate relation $\mathbf{R}=\mathbf{N}^+=\mathbf{J}$ can be used to label the ionic levels. Moreover, in a general effective Hamiltonian, the coefficients of the various terms are defined from the expectation values of the electronic and vibrational angular momentum operators over the vibronic functions, but the evaluation of such functions in the full-dimensional problem still represents a considerable challenge. In our effective Hamiltonian (13), these coefficients are simple linear combinations of the rotational constants. Therefore we use Hamiltonian (13) in the following analysis, although we realize that it only provides accurate results in situations where the wave function is strongly localized in the minima and the tunneling motion is slow on the time scale of molecular rotation.

IV. RESULTS

A. Correlation diagram

The properties of the tunneling-rotation Hamiltonian derived in Eq. (13) are most easily understood in terms of the correlation diagram presented in Fig. 5. In this figure, the eigenvalues of $\hat{H}_{\mathrm{rve}}$ for the total angular momentum quantum number excluding spins $N^+=0-3$ calculated using the rotational constants A,B,C derived in Ref. 1 are represented as a function of the tunneling integral $\sigma=\delta/4$. The case $\sigma=0$ corresponds to a situation where tunneling is suppressed by infinite barriers between the minima or, equivalently, the vibronic wave functions are completely localized in the minima of C_{2v} geometry. This situation results in the level structure of an asymmetric top molecule with rotational constants A, B, and C, in which each level is sixfold degenerate. The value of J is indicated on the left-hand side of the figure. In the case of a nonzero tunneling splitting δ, the sixfold degeneracy of each asymmetric top level is lifted, and the levels can be assigned a rovibronic symmetry Γ_{rve} in the $T_d(M)$ molecular symmetry group (A_1, A_2, E, F_1, or F_2). In the case of a vanishing barrier, which corresponds to nearly free pseudorotation, the eigenvalues of $\hat{H}_{\mathrm{rve}}$ form two distinct stacks of rotational levels corresponding to two states of vibronic symmetries F_2 and F_1, respectively. The rotational structure in this limit does not correspond to a simple symmetric or asymmetric top, but the splittings between levels of the same J quantum number are smaller than in the asymmetric top limit which we attribute to the effects of pseudorotational averaging. Overall the grouping of levels is reminiscent of the rotational structure of a spherical top. One cannot, however, expect that the level structure in this limiting case is accurately predicted because the pseudorotational motion generates angular momentum that couples to the rotational angular momentum and these Coriolis interactions are not included in $\hat{H}_{\mathrm{rve}}$. Moreover, the assumption of a strong localization of the vibronic functions in the minima is

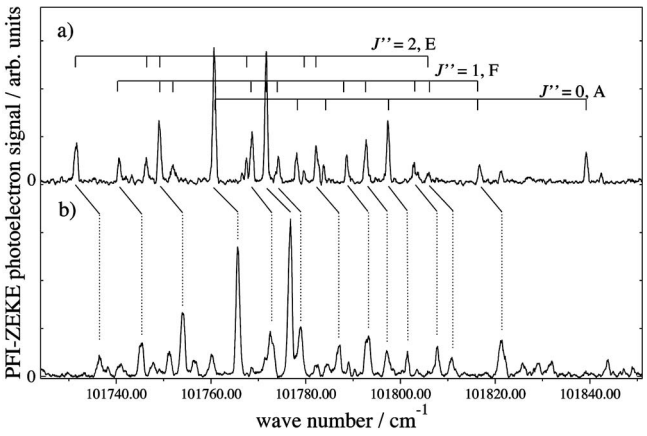

FIG. 6. Single-photon PFI-ZEKE photoelectron spectrum of $^{13}CH_4$ [bottom trace, (b)] and $^{12}CH_4$ [top trace, (a)] in the region of the adiabatic ionization threshold. Spectrum (a) was obtained with a sequence of pulsed electric fields of +26 and −138 mV cm^{-1} and spectrum (b) with +26 and −88 mV cm^{-1}.

no longer adequate and the tunneling model for the pseudorotational motion is expected to break down.

The rovibronic symmetries indicated in Fig. 5 have been derived directly from the calculation, but they can also be obtained from group theoretical arguments. In the case $\delta=0$, all levels can be assigned to a rovibronic symmetry in the C_{2v} point group. The correlation to the $T_d(M)$ molecular symmetry group provides the rovibronic symmetries of the levels into which the asymmetric top levels split as a result of tunneling. This procedure is illustrated for the $J=1$ levels in Fig. 5. Their rovibronic symmetries are $B_1(J_{K_aK_c}=1_{01})$, $A_1(1_{11})$, and $A_2(1_{10})$, which correlate with $F_1 \oplus F_2$, $A_1 \oplus E \oplus F_2$, and $A_2 \oplus E \oplus F_1$, respectively. As can be seen from Fig. 5, the rovibronic symmetries are correctly predicted from the diagonalization of $\hat{H}_{\mathrm{rve}}$.

B. PFI-ZEKE photoelectron spectra

The rotationally resolved PFI-ZEKE photoelectron spectra of $^{13}CH_4$, $^{12}CH_4$, and $^{12}CD_4$ recorded following one-photon VUV excitation are shown in Figs. 6–8. The coincidence of the observed bands with a sharp onset of the photoionization signal (not shown) and the absence of PFI-ZEKE photoelectron signal at lower wave numbers provide strong evidence for the assignment of these bands to the origin of the photoelectron spectra (see also discussion in Ref. 10). The spectra of CH_4 and $^{13}CH_4$ have linewidths of 0.5 and 0.8 cm^{-1}, respectively, in good agreement with the linewidth expected from the electric field sequences used to record them.[36] Most lines in the spectra of $^{13}CH_4$ and CH_4 correspond to transitions between a single pair of rotational levels. The PFI-ZEKE photoelectron spectrum (Fig. 8) of CD_4^+ has a much lower signal-to-noise ratio than those of CH_4^+ and $^{13}CH_4^+$. Moreover, the linewidth in this spectrum amounts to 0.7–1.2 cm^{-1}, more than the value of 0.6 cm^{-1} expected from the pulsed electric field sequence. Thus, most observed lines correspond to several transitions.

If a small isotopic shift indicated by diagonal lines in Fig. 6 is excepted, the PFI-ZEKE spectra of $^{12}CH_4$ and $^{13}CH_4$ are very similar. The main transitions are grouped according to the ground state level on the basis of the assignment procedure discussed in more detail in Sec. IV B 1.

The analysis of the rotational structure in the spectrum of CH_4^+ with standard rigid rotor Hamiltonians has not been successful, a finding that has been attributed to the fluxional nature of the methane cation.[9,10] An additional difficulty in the analysis resulted from the fact that no combination differences could be identified in the spectra which prevented the assignment of the initial level of the transitions. The reason for the absence of combination differences lies in the fact that the methane molecules are cooled to the lowest rotational level of each nuclear spin symmetry in the supersonic expansion, i.e., $J=0$ for nuclear spin symmetry A_1, $J=1$ for F_2, and $J=2$ for E, as already pointed out in Sec. II (see Fig. 1). For these reasons, an experimental assignment of nuclear spin symmetry in the spectrum of CH_4^+ was necessary.

1. CH_4^+

The assignment of the rovibronic symmetries of the ionic levels observed in the PFI-ZEKE photoelectron spectrum is a prerequisite to its analysis with the effective Hamiltonian $\hat{H}_{\mathrm{rve}}$. Two double-resonance techniques have been developed to assign the nuclear spin symmetries of the ionic

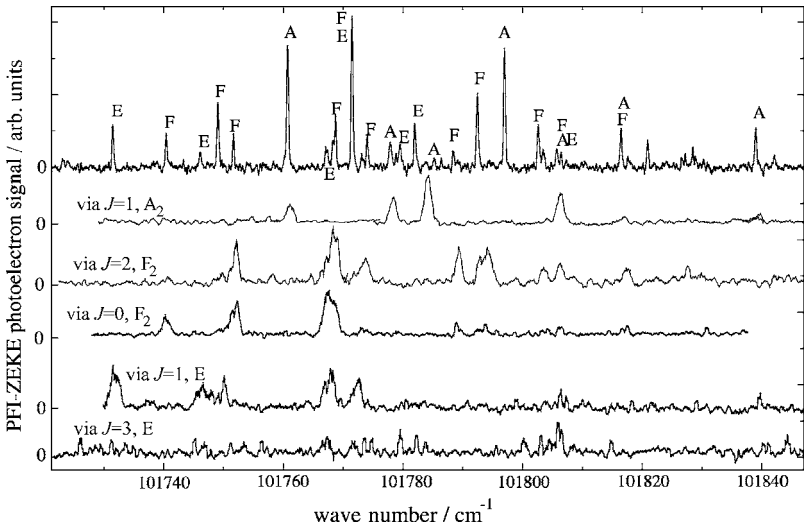

FIG. 7. Top trace: single-photon PFI-ZEKE photoelectron spectrum of CH_4 in the region of the adiabatic ionization threshold obtained using electric field pulses of +86 and −138 mV cm^{-1}. Lower traces: two-photon IR+VUV PFI-ZEKE PE spectra recorded via selected rotational levels of the ν_3 fundamental using electric field pulses of +17 and −860 mV cm^{-1}. The rotational angular momentum quantum number J of the intermediate levels and their rovibronic symmetries are indicated above the spectra. The letters A, E, and F correspond to the experimentally assigned nuclear spin symmetries (A_1, E, and F_2).

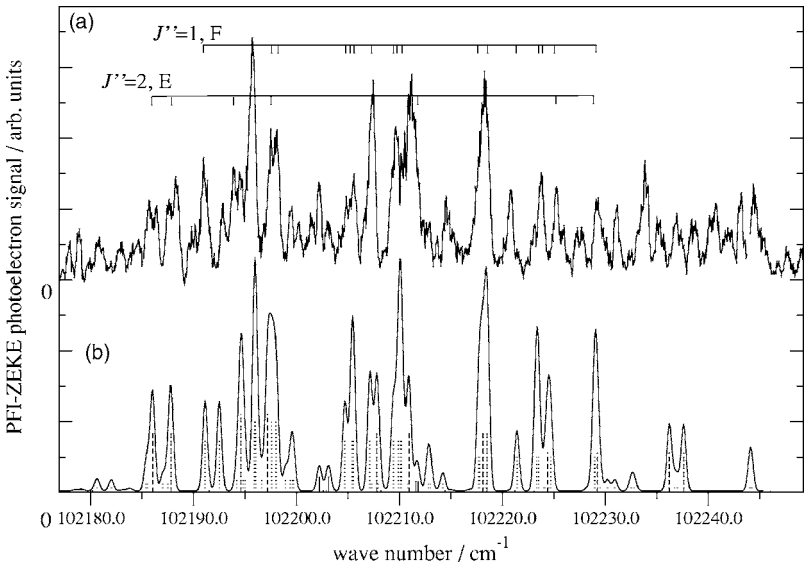

FIG. 8. Single-photon PFI-ZEKE photoelectron spectrum of CD_4 in the region of the adiabatic ionization threshold (a) obtained using a pulsed electric field of $-53\ \mathrm{mV\,cm^{-1}}$ and simulated spectrum using Hamiltonian (13) and the constants indicated in Table VI (b). Panel (b) shows a theoretical stick spectrum and its convolution with a Gaussian line profile of FWHM of $0.55\ \mathrm{cm^{-1}}$. The full, dashed, and dotted sticks represent transitions to levels of rovibronic symmetries A_1 (or A_2), E, and F_1 (or F_2), respectively.

levels, and the first results were reported in Ref. 1. First, the depletion of the PFI-ZEKE photoelectron signal was monitored as a function of the IR radiation frequency that was chosen to be resonant with the $R(0)$, $P(1)$, $R(1)$, $P(2)$, or $R(2)$ lines of the ν_3 fundamental band. A depletion of up to $\approx 50\%$ of the original signal indicated that the photoionizing and IR transitions had a common lower level. Second, PFI-ZEKE spectra were recorded from selected rotational levels of the $\upsilon_3=1$ vibrationally excited state of neutral methane following IR excitation. The results obtained from these two methods are displayed in Fig. 7. The top trace of Fig. 7 represents the single-photon PFI-ZEKE photoelectron spectrum of CH_4 that was recorded at an experimental resolution of $0.36\ \mathrm{cm^{-1}}$. The lower traces represent IR+VUV two-photon resonant PFI-ZEKE photoelectron spectra recorded via selected rotational levels of the intermediate $\upsilon_3=1$ vibrationally excited level of CH_4. The rovibronic symmetry label and the rotational angular momentum quantum number J of the intermediate level are indicated above each trace. The wave number scale corresponds to the sum of the IR and the VUV wave numbers. The linewidth in the IR+VUV two-photon spectra amounts to approximately $1\ \mathrm{cm^{-1}}$, limited by the amplitude of the pulsed ionization field which had to be chosen larger than in the one-photon experiments because of weaker signals. The coincidence of a PFI-ZEKE line in the single-photon and two-photon spectra (after field correction) was used to assign a nuclear spin symmetry to the ionic levels. Combining the results of the "ZEKE dip" and two-photon resonant PFI-ZEKE spectra, nuclear spin symmetries could be assigned to most lines in the PFI-ZEKE photoelectron spectrum and the map of the lowest rovibronic levels of the methane cation shown in Fig. 9(a) could be established.

A nonlinear least-squares fitting procedure of the eigenvalues of $\hat{H}_{\mathrm{rve}}$ to the experimental level positions provided the constants given in Table VI, and Fig. 9(b) shows the level structure calculated with the Hamiltonian $\hat{H}_{\mathrm{rve}}$. Table VII summarizes observed and calculated level positions and the spectral assignments. The value of the ionization energy differs slightly from the value reported in Ref. 1 because of a

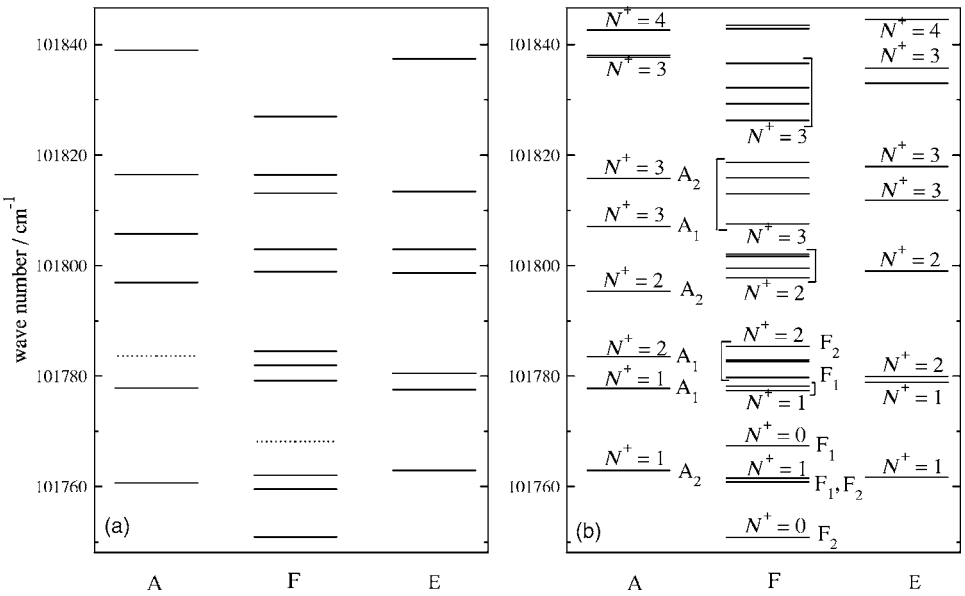

FIG. 9. Comparison of the experimentally determined level structure of CH_4^+ (a) with the eigenvalues of Hamiltonian (13) calculated using the constants determined in a nonlinear least-squares fitting procedure (b). The wave number scale is defined with respect to the ground state of CH_4.

TABLE VI. Adiabatic ionization energy, rotational constants (A,B,C), and tunneling splitting δ determined from a least-squares fitting procedure of the calculated to the observed line positions for CH_4^+, $^{13}CH_4^+$, and CD_4^+.

Constant (cm^{-1})	IE/hc	A	B	C	δ
CH_4^+	101 752.2(15)	6.40(50)	5.55(40)	4.03(50)	16.4(40)
$^{13}CH_4^+$	101 756.6(15)	6.30(50)	5.70(45)	4.05(40)	16.2(40)
CD_4^+	102 196.9(15)	3.35(30)	2.53(25)	1.98(20)	1.4(3)

more accurate estimation of the field-induced shift of the ionization thresholds. The two values agree within their uncertainty.

2. $^{13}CH_4^+$

The PFI-ZEKE photoelectron spectrum of $^{13}CH_4$ has been recorded under conditions similar to those used for $^{12}CH_4$ but using a slightly higher pulsed electric field as indicated in the figure caption. Except from a shift of +4.4 cm^{-1} of the spectrum of $^{13}CH_4$ with respect to that of CH_4, the two spectra are very similar in appearance. No major differences are observed in the intensity distributions except for the region around 101 800 cm^{-1}, where the relative intensities of several lines differ. Also, a few additional lines are observed in the spectrum of $^{13}CH_4$ at 101 760.05, 101 747.65, 101 828.97, and 101 831.72 cm^{-1}. The great similarity of the lowest band of the PFI-ZEKE photoelectron spectra of $^{12}CH_4^+$ and $^{13}CH_4^+$ is not surprising given that neither the rotational constants nor the pseudorotational tunneling dynamics are expected to be significantly affected by the substitution of the central atom. The observed and calculated positions of the lines observed in the PFI-ZEKE photoelectron spectrum of $^{13}CH_4^+$ are listed in Table VIII which also contains the spectral assignments. The constants obtained in the nonlinear least-squares fit are listed in Table VI.

3. CD_4^+

Figure 8(a) shows the PFI-ZEKE photoelectron spectrum of CD_4 and Fig. 8(b) shows a simulation using the effective tunneling-rotation Hamiltonian of Eq. (13). The signal-to-noise ratio of the experimental spectrum is significantly lower than in the case of the PFI-ZEKE spectra of CH_4, although the spectra were recorded under similar conditions. Since the photoelectron transitions in the region of

TABLE VII. Measured line positions ($\tilde{\nu}_{obs}$) and deviations from the calculated line positions ($\tilde{\nu}_{obs}-\tilde{\nu}_{calc}$) of the vibrationless CH_4^+ $\tilde{X}\leftarrow CH_4$ $\tilde{X}$ photoionizing transition. Γ_{ve}, Γ_{ve}^+ and Γ_{rve}, Γ_{rve}^+ represent the vibronic and the rovibronic symmetries in the molecular symmetry group $T_d(M)$ for the neutral and the ionic states, respectively. The distinction between A_1 and A_2 or F_1 and F_2 was not always possible.

CH_4 ($\Gamma_{ve}=A_1$)		CH_4^+ ($\Gamma_{ve}^+=F_2,F_1$)			
J	Γ_{rve}	N^+	Γ_{rve}^+	$\tilde{\nu}_{obs}$ (cm^{-1})[a]	($\tilde{\nu}_{calc}-\tilde{\nu}_{obs}$) ($cm^{-1}$)
2	E	1	E	101 731.49	−1.27
1	F_1	0	F_2	101 740.44	0.00[b]
2	E	1	E	101 746.11	1.32
1	F_1	1	F	101 749.08	1.30
2	E	2	E	101 749.08	−0.78
1	F_1	1	F	101 751.64	−0.59
0	A_1	1	A_2	101 760.71	2.11
2	E	2	E	101 767.26	0.09
1	F_1	2	F_1	101 768.70	−0.60
1	F_1	2	F	101 771.49	−0.70
2	E	2/3	E	101 771.49	
1	F_1	2	F_2	101 774.05	−0.83
0	A_1	1	A_1	101 777.88	−0.16
2	E	3	E	101 782.01	
2	E	3/4	E	101 805.94	
0	A_1	2	A_1	101 783.64	−0.31
1	F_1	2	F	101 788.43	0.51
1	F_1	2	F	101 792.49	−1.09
0	A_1	2	A_2	101 797.00	−1.78
1	F_1	3	F	101 802.63	−0.45
0	A_1	3	A_1	101 805.74	1.00
0	A_1	3	A_2	101 816.49	−0.95
1	F_1	3	F	101 816.49	−1.00
0	A_1	3/4	A	101 839.23	

[a]Measured transitions without field correction.
[b]Band origin.

TABLE VIII. Measured line positions ($\tilde{\nu}_{obs}$) and deviations from the calculated line positions ($\tilde{\nu}_{obs}-\tilde{\nu}_{calc}$) of the vibrationless $^{13}CH_4^+$ $\tilde{X}\leftarrow{}^{13}CH_4$ $\tilde{X}$ photoionizing transition. Γ_{ve}, Γ_{ve}^+ and Γ_{rve}, Γ_{rve}^+ represent the vibronic and the rovibronic symmetries in the molecular symmetry group $T_d(M)$ for the neutral and the ionic states, respectively. The distinction between A_1 and A_2 or F_1 and F_2 was not always possible.

$^{13}CH_4$ ($\Gamma_{ve}=A_1$)		$^{13}CH_4^+$ ($\Gamma_{ve}^+=F_2,F_1$)			
J	Γ_{rve}	N^+	Γ_{rve}^+	$\tilde{\nu}_{obs}$ (cm^{-1})[a]	($\tilde{\nu}_{calc}-\tilde{\nu}_{obs}$) ($cm^{-1}$)
2	E	1	E	101 736.52	−1.49
1	F_1	0	F_2	101 745.26	0.00[b]
2	E	1	E	101 751.19	0.95
1	F_1	1	F	101 754.05	+1.26
1	E	2	E	101 754.05	−0.55
1	F_1	1	F	101 756.48	−0.41
0	A_1	1	A_2	101 765.68	2.07
2	E	2	E	101 772.56	0.15
1	F_1	2	F_1	101 772.56	1.69
1	F_1	2	F	101 776.72	0.56
2	E	2/3	E	101 776.72	
1	F_1	2	F_2	101 778.83	1.17
0	A_1	1	A_1	101 782.26	0.05
2	E	3	E	101 784.58	
2	E	3/4	E	101 786.95	
0	A_1	2	A_1	101 789.03	−0.09
1	F_1	2	F	101 793.08	−1.03
1	F_1	2	F	101 797.25	−0.81
0	A_1	2	A_2	101 801.45	−1.28
1	F_1	3	F	101 807.75	−0.16
0	A_1	3	A_1	101 810.81	1.14
0	A_1	3	A_2	101 821.34	−0.47
0	A_1		A	101 843.71	

[a]Measured transitions without field correction.
[b]Band origin.

the adiabatic ionization threshold of CD_4^+ are considerably weaker than in CH_4 and only few individual transitions are resolved, an experimental assignment based on the double-resonance schemes described above was not undertaken for CD_4^+. In a previous analysis of the PFI-ZEKE spectrum of CD_4,[10] it was argued that the tunneling splitting was smaller than the spectral resolution and that the spectrum could be analyzed with an asymmetric top Hamiltonian. A reanalysis of the spectrum with the Hamiltonian $\hat{H}_{rve}$ derived in the present work, however, leads to the conclusion that an adjustment of the rotational constants A,B,C, the tunneling splitting δ, and the ionization energy IE leads to a better agreement between the experimental and theoretical spectra. In particular, the tunneling splitting is determined to be 1.4(3) cm^{-1}. The constants obtained in a nonlinear least-squares fitting procedure are given in Table VI. Table IX summarizes observed and calculated level positions and the spectral assignments. The positions of the transitions have been calculated using the rotational constant $B=2.63273$ cm^{-1} (Ref. 47) for the ground state of CD_4 and assuming that the nuclear spin symmetry is conserved in the photoionizing transition. The simulation of intensities was performed assuming a Boltzmann distribution of the neutral ground state levels at 7 K for each nuclear spin symmetry. The simulations also include the spatial degeneracies $(2J+1)$ of the lower levels of the transitions, the spin-statistical weights, and the same weighting factors for the different rotational branches $C_{\Delta N}$ ($C_0=1$, $C_1=C_{-1}=0.75$, $C_2=C_{-2}=0.50$) as already successfully used in the simulation of the spectrum of $CH_2D_2^+$.[11] The transitions corresponding to the emission of a photoelectron with even or odd parity were weighted equally. Figure 8(b) shows a calculated stick spectrum and a convolution with a Gaussian envelope of full width at half maximum (FWHM) of 0.55 cm^{-1}.

The agreement between simulated and observed spectra in Fig. 8 is good as far as the line positions are concerned and satisfactory as far as the intensities are concerned. All strong features in the spectrum are reproduced well, especially on the low energy side of the spectrum. The effect of the tunneling splitting is most pronounced in the group of transitions originating from $J=1$ at 102 195.6 and 102 197.8 cm^{-1}. If a rigid asymmetric top model is used, this pair of lines must be assigned to the transitions from $J=1$ to $N^+_{K_aK_c}=1_{01},1_{11},1_{10}$, respectively, where J designates the total angular momentum quantum number of the initial neutral level, and N^+, K_a, K_c the rotational angular momentum quantum number and its prolate and oblate top projections.[10] These final states are almost equally spaced and equally intense, in contrast to the observation. The introduction of a tunneling splitting of 1.4 cm^{-1} moves the components of nuclear spin symmetry F_2 of the upper two levels to higher energies and leads to a splitting of the lower level in two components, which agrees very well with the observed structure. It also improves the agreement with the measured spec-

TABLE IX. Measured line positions ($\tilde{\nu}_{obs}$) and deviations from the calculated line positions ($\tilde{\nu}_{obs}-\tilde{\nu}_{calc}$) of the vibrationless $CD_4^+ \tilde{X} \leftarrow CD_4 \tilde{X}$ photoionizing transition. Γ_{ve}, Γ_{ve}^+ and Γ_{rve}, Γ_{rve}^+ represent the vibronic and the rovibronic symmetries in the molecular symmetry group $T_d(M)$ for the neutral and the ionic states, respectively. The distinction between F_1 and F_2 was not always possible.

CD_4 ($\Gamma_{ve}=A_1$)		CD_4^+ ($\Gamma_{ve}^+=F_2,F_1$)			
J	Γ_{rve}	N^+	Γ_{rve}^+	$\tilde{\nu}_{obs}$ (cm^{-1})[a]	($\tilde{\nu}_{calc}-\tilde{\nu}_{obs}$) ($cm^{-1}$)
0	A_1	1	A_2	102 202.2	0.02
1	F_1	0	F_2	102 191.0	0.08
1	F_1	1	F	102 195.7	0.19
1	F_1	1	F	102 195.7	0.30
1	F_1	1	F_1	102 197.8	–0.25
1	F_1	1	F_2	102 197.8	0.18
1	F_1	2	F_1	102 207.3	–0.21
1	F_1	2	F	102 209.6	–0.19
1	F_1	3	F	102 218.2	–0.44
1	F_1	3	F	102 218.2	–0.38
1	F_1	3	F	102 218.2	0.26
1	F_1	3	F	102 220.8	0.57
1	F_1	3	F	102 223.7	–0.15
2	E	1	E	102 185.9	0.08
2	E	1	E	102 188.0	–0.24
2	E	2	E	102 207.3	0.49
2	E	2	E	102 211.2	–0.31
2	E	3	E	102 218.2	–0.11
2	E	3	E	102 218.2	0.21

[a]Measured transitions without field correction.

trum in the lowest wave number region, where the pair of transitions at 102 186 and 102 188 cm^{-1} is reproduced quantitatively.

V. DISCUSSION

A. Comparison of experimental and simulated spectra

The agreement between calculated and observed level positions is satisfactory in CH_4^+ and good in CD_4^+. In CH_4^+ a one-to-one correspondence between the calculated and experimental level positions of nuclear spin symmetries A_1 and E is found up to $N^+=3$. More levels of nuclear spin symmetry F_2 have been calculated than observed which is most likely a result of the limited resolution and sensitivity of the experiment. However, the grouping of calculated levels closely reflects the experimental results. In CD_4^+, an experimental assignment of the nuclear spin symmetries was not required because the experimental spectrum could be assigned on the basis of the calculation. However, the lower signal-to-noise ratio of the CD_4 spectrum and the higher spectral congestion make a comparison more difficult than in the case of CH_4^+. The rotational constants obtained in the analysis of the spectra of CH_4^+ and CD_4^+ are both consistent with the experimental geometry derived from the PFI-ZEKE spectra of $CH_2D_2^+$.[11]

The tunneling splittings obtained from the present analysis are significantly larger than those obtained from one-dimensional calculations of the pseudorotational motion,[10] but they are in agreement with the results of ESR spectra which have shown that the exchange of hydrogen atoms takes place on a subnanosecond time scale.[5] In early *ab initio* calculations[15,16] the barrier height depended strongly on the methods used and/or the representation of the potential surface. More recent calculations seem to converge to a purely electronic barrier height of approximately 1000 cm^{-1}.[10,17] However, zero-point corrections must be added to this electronic value, which is not straightforward in highly anharmonic potential surfaces.

Ab initio calculations at the CCSD(T)/cc-pVTZ level of theory provide harmonic zero-point energies of 8398 and 6156 cm^{-1} at the C_{2v} minimum for CH_4^+ and CD_4^+, respectively. At the C_s saddle point corresponding to the pseudorotational motion, the zero-point energies amount to 7782 and 5673 cm^{-1}, respectively. The purely electronic barrier amounts to 1014 cm^{-1} at this level of theory. The zero-point corrected barrier amounts to only 399 cm^{-1} for CH_4^+ and 530 cm^{-1} for CD_4^+. Zero-point effects thus strongly reduce the size of this barrier which explains the large value of the tunneling splitting of 16(4) cm^{-1} for CH_4^+ which corresponds to a period of 2.1(5) ps for the exchange of hydrogen atoms.

A striking difference between the PFI-ZEKE spectra of CH_4^+ and CD_4^+ is the much lower signal-to-noise ratio in the CD_4^+ spectra. The simplest explanation of this observation can be given in terms of a Franck-Condon argument.[10] The Franck-Condon factor depends on the amplitude of the ionic nuclear wave function in the vicinity of the tetrahedral geometry of the neutral molecule. As a consequence of deuteration, the zero-point energy of the lowest levels is reduced which results in a stronger localization of the wave function in the regions of the potential surface corresponding to the distorted structures. Consequently, the amplitude of the vibronic wave function in the Franck-Condon region of the

photoionizing transition is decreased by deuteration which results in significantly weaker transitions in CD_4^+ than in CH_4^+.

B. Thermochemical implications

The present work has improved the accuracy in the ionization energy of methane by a factor of more than 20. This ionization energy is an important thermochemical quantity and several consequences are discussed. Since the appearance energy (AE) of CH_3^+ from the photoionization of methane $AE(CH_3^+,CH_4)$ is known accurately,[48] the 0 K bond dissociation energy $D_0(H-CH_3^+)$ can be determined to high accuracy

$$D_0(CH_3^+ - H) = AE(CH_3^+,CH_4) - IE(CH_4) = 13\,769.7 \pm 8\ cm^{-1}. \quad (16)$$

Upon ionization, the C–H bond of methane is thus weakened and the dissociation energy decreases by a factor of almost 3. A comparison of the appearance energy $AE(CH_3^+,CH_4)$ of $115\,522.7 \pm 8\ cm^{-1}$ (Ref. 48) with the sum $(115\,528.4\ cm^{-1})$ of the ionization energy of the methyl radical $79\,356.4 \pm 1.5\ cm^{-1}$ (Ref. 49) and the bond dissociation energy $D_0(H-CH_3)$ $36172 \pm 10\ cm^{-1}$ shows that the dissociation of CH_4^+ into a methyl cation and a hydrogen atom is barrierless within the accuracy of these measurements.

The dissociation of methane cation into CH_2^+ and H_2 is another important process. Using the ionization energy $IE(CH_2) = 83772 \pm 3\ cm^{-1}$ of CH_2 (Ref. 50) and the 0 K dissociation energy $D_0(CH_2-H_2)$ of methane into CH_2 and H_2 improved in Ref. 50, one obtains the 0 K dissociation energy of CH_4^+ into CH_2^+ and H_2

$$D_0(CH_2^+ - H_2) = D_0(CH_2 - H_2) + IE(CH_2) - IE(CH_4) = 20\,251 \pm 50\ cm^{-1}. \quad (17)$$

In this evaluation, the sum of the dissociation energy of neutral methane $(38\,232 \pm 50\ cm^{-1})$ and the ionization energy of methylene $(83\,772 \pm 3\ cm^{-1})$ have been used because it is smaller than the appearance energy of CH_2^+ from the photoionization of CH_4 $AE(CH_2^+,CH_4) = 122\,274\ cm^{-1}$ (Ref. 51) by $270\ cm^{-1}$, which suggests the existence of a barrier for the dissociation of CH_4^+ into CH_2^+ and H_2.

VI. CONCLUSIONS

The assignment of the origin band in the spectra of CH_4^+, $^{13}CH_4^+$, and CD_4^+ in terms of a tunneling doublet of vibronic symmetries F_2 and F_1 in $T_d(M)$ confirms the C_{2v} minimum energy geometry of CH_4^+ and CD_4^+ that results from the JT effect. C_{3v} and D_{2d} geometries would result in different tunneling structures as discussed in Sec. III C and can be excluded. A model of the pseudorotation-tunneling dynamics has been developed that enables the interpretation of the irregular and complex spectral structures observed in the photoelectron spectra. The model can be used to explore the diversity of behaviors between the free pseudorotation and complete localization of the nuclear structure in the C_{2v} minima by means of a correlation diagram. Deviations between measured and predicted level positions amount to about $1\ cm^{-1}$ for CH_4^+ and $0.3\ cm^{-1}$ for CD_4^+. We attribute the better prediction of the CD_4^+ spectrum to the stronger localization in the C_{2v} potential wells. The present characterization of level positions and symmetries represents an important step toward the observation of the millimeter wave spectrum of CH_4^+. We indeed expect transitions between rotational levels of different tunneling components of the same nuclear spin symmetry to be observable.

ACKNOWLEDGMENTS

The authors thank R. van der Veen for her contributions to the theoretical analysis in the early phase of the project. This work is supported financially by the Swiss National Science Foundation and the ETH Zürich.

[1] H. J. Wörner, R. van der Veen, and F. Merkt, Phys. Rev. Lett. **97**, 173003 (2006).
[2] D. Luckhaus, J. Chem. Phys. **113**, 1329 (2000).
[3] X. G. Wang and T. Carrington, J. Chem. Phys. **119**, 101 (2003).
[4] L. B. Knight, Jr., J. Steadman, D. Feller, and E. R. Davidson, J. Am. Chem. Soc. **106**, 3700 (1984).
[5] L. B. Knight, Jr., G. M. King, J. T. Petty, M. Matsushita, T. Momose, and T. Shida, J. Chem. Phys. **103**, 3377 (1995).
[6] M. Matsushita, T. Momose, T. Shida, and L. B. Knight, Jr., J. Chem. Phys. **103**, 3367 (1995).
[7] J. W. Rabalais, T. Bergmark, L. O. Werme, L. Karlsson, and K. Siegbahn, Phys. Scr. **3**, 13 (1971).
[8] A. W. Potts and W. C. Price, Proc. R. Soc. London, Ser. A **326**, 165 (1972).
[9] R. Signorell and F. Merkt, J. Chem. Phys. **110**, 2309 (1999).
[10] R. Signorell and F. Merkt, Faraday Discuss. **115**, 205 (2000).
[11] R. Signorell, M. Sommavilla, and F. Merkt, Chem. Phys. Lett. **312**, 139 (1999).
[12] W. Meyer, J. Chem. Phys. **58**, 1017 (1973).
[13] J. Arents and L. C. Allen, J. Chem. Phys. **53**, 73 (1970).
[14] R. N. Dixon, Mol. Phys. **20**, 113 (1971).
[15] M. N. Paddon-Row, D. J. Fox, J. A. Pople, K. N. Houk, and D. W. Pratt, J. Am. Chem. Soc. **107**, 7696 (1985).
[16] R. F. Frey and E. R. Davidson, J. Chem. Phys. **88**, 1775 (1988).
[17] S. Zilberg and Y. Haas, J. Am. Chem. Soc. **125**, 1810 (2003).
[18] K. Takeshita, J. Chem. Phys. **86**, 329 (1987).
[19] F. Marinelli and M. Roche, Chem. Phys. **146**, 219 (1990).
[20] M. S. Reeves and E. R. Davidson, J. Chem. Phys. **95**, 6551 (1991).
[21] R. Signorell and M. Sommavilla, J. Electron Spectrosc. Relat. Phenom. **108**, 169 (2000).
[22] U. Öpik and M. H. L. Pryce, Proc. R. Soc. London, Ser. A **238**, 425 (1957).
[23] I. B. Bersuker and V. Z. Polinger, Sov. Phys. JETP **39**, 1023 (1974).
[24] I. B. Bersuker, *The Jahn-Teller Effect* (Cambridge University Press, Cambridge, 2006).
[25] M. Keil, H.-G. Krämer, A. Kudell, M. A. Baig, J. Zhu, W. Demtröder, and W. Meyer, J. Chem. Phys. **113**, 7414 (2000).
[26] H. von Busch, V. Dev, H.-A. Eckel, S. Kasahara, J. Wang, W. Demtröder, P. Sebald, and W. Meyer, Phys. Rev. Lett. **81**, 4584 (1998). See also erratum (Ref. 28).
[27] D. T. Vituccio, O. Golonzka, and W. E. Ernst, J. Mol. Spectrosc. **184**, 237 (1997).
[28] H. von Busch, V. Dev, H.-A. Eckel, S. Kasahara, J. Wang, W. Demtröder, P. Sebald, and W. Meyer, Phys. Rev. Lett. **82**, 3560(E) (1999).
[29] N. Ohashi, M. Tsuura, J. T. Hougen, W. E. Ernst, and S. Rakowsky, J. Mol. Spectrosc. **184**, 22 (1997).
[30] M. Mayer and L. Cederbaum, J. Chem. Phys. **105**, 4938 (1996).
[31] F. Merkt, A. Osterwalder, R. Seiler, R. Signorell, H. Palm, H. Schmutz, and R. Gunzinger, J. Phys. B **31**, 1705 (1998).
[32] A. H. Kung, S. Fei, and H. L. Strauss, Appl. Spectrosc. **50**, 790 (1996).
[33] T. Momose, T. Wakabayashi, and T. Shida, J. Opt. Soc. Am. B **13**, 1706 (1996).
[34] B. Bobin, J. Phys. (France) **33**, 345 (1972).
[35] *Wavelengths by Element*, M.I.T. Wavelength Tables Vol. 2, edited by F. M. Phelps III (MIT Press, Cambridge, MA, 1982).

[36] U. Hollenstein, R. Seiler, H. Schmutz, M. Andrist, and F. Merkt, J. Chem. Phys. **115**, 5461 (2001).
[37] M. J. M. Pepper, I. Shavitt, P. von Ragué Schleyer, M. N. Glukhovtsev, R. Janoschek, and M. Quack, J. Comput. Chem. **16**, 207 (1995).
[38] M. Quack, Angew. Chem., Int. Ed. Engl. **28**, 571 (1989).
[39] P. R. Bunker and P. Jensen, *Molecular Symmetry and Spectroscopy* (NRC Research, Ottawa, 1998).
[40] M. Quack, Mol. Phys. **34**, 477 (1977).
[41] J. T. Hougen and N. Ohashi, J. Mol. Spectrosc. **109**, 134 (1985).
[42] F. S. Ham, Phys. Rev. **138**, A1727 (1965).
[43] F. S. Ham, J. Phys.: Condens. Matter **2**, 1163 (1990).
[44] C. P. Moate, M. C. M. O'Brien, J. L. Dunn, C. A. Bates, Y. M. Liu, and V. Z. Polinger, Phys. Rev. Lett. **77**, 4362 (1996).
[45] H. Koizumi, I. B. Bersuker, J. E. Boggs, and V. Z. Polinger, J. Chem. Phys. **112**, 8470 (2000).
[46] M. S. Child and H. C. Longuet-Higgins, Philos. Trans. R. Soc. London, Ser. A **254**, 259 (1961).
[47] J. E. Lolck, G. Poussigue, E. Pascaud, and G. Guelachvili, J. Mol. Spectrosc. **111**, 235 (1985).
[48] K. M. Weitzel, M. Malow, G. K. Jarvis, T. Baer, Y. Song, and C. Y. Ng, J. Chem. Phys. **111**, 8267 (1999).
[49] A. M. Schulenburg, Ch. Alcaraz, G. Grassi, and F. Merkt, J. Chem. Phys. **125**, 104310 (2006).
[50] S. Willitsch, A. Haldi, and F. Merkt, Chem. Phys. Lett. **353**, 167 (2002).
[51] K. E. McCulloh and V. H. Dibeler, J. Chem. Phys. **64**, 4445 (1976).